Ocean Engineering 218 (2020) 108121

Contents lists available at ScienceDirect

Ocean Engineering

journal homepage: www.elsevier.com/locate/oceaneng

Formulation of wave and current forces acting on a body and resistance of ships

S. Beji

Faculty of Naval Architecture and Ocean Engineering, Istanbul Technical University, Maslak, 34469, Istanbul, Turkey

ARTICLE INFO

Keywords:
Wave and current forces
Inertia drag and frictional forces
Morison's equation
Ship resistance

ABSTRACT

A general expression is formulated from the first principles for wave and current forces acting on a body. Morison's equation is recovered as a special case of the general formulation, thus establishing this heuristic-regarded equation on a firm theoretical ground. The drag force is clearly seen to be originating from the advective acceleration and the skin friction resistance, which is not explicitly represented in Morison's equation, is viewed as a small part of the drag force. For the special case of constant flow velocity the general expression is employed to derive a resistance formula for ships. The viscous term is handled through the use of Prandtl-Kármán formulation of friction drag due to a turbulent boundary layer. Conflict between Froude and Reynolds scaling is reconciled by allowing a deviation from the true partition of the corresponding forces but ensuring in return the correct scaling of the total resistance force for the model and ship. The performance of the resistance formula is checked against the experimental measurements of various ship forms. Finally, formulas for forces due to a current at an angle to a ship are suggested.

1. Introduction

Estimation of forces acting on an object moving in fluid or fixed in space but subjected to a flow field has always been of a major interest to engineers. Froude (Froude and Froude, 1888) made the first comprehensive and practical treatment of ship resistance and set the tone for further research on this subject. As to the wave forces acting on a fixed object, the work of Morison, O'Brien, Johnson, and Scaaf (Morison et al., 1950) in 1950, which resulted in the formulation known briefly as the Morison equation, may be referred to as pioneering and most widely used one. Despite its popularity this formulation has been regarded as a heuristic expression combining the inertia and drag forces. Indeed, the paper opens by simply stating the formulation without embarking on any justifying argument. The total force exerted by surface waves is simply pronounced as composed of a virtual mass force and a drag force. This distinct separation and subsequent addition of these different contributions have often been questioned (Sarpkaya and Isaacson, 1981; SPM, 1984). Here, it is not only observed clearly that these two forces essentially stem from the same source but also their addition is naturally dictated by the momentum equation itself. Furthermore, a third contribution arising from the frictional effects is identified and expressed in terms of mean flow velocity as formulated by Prandtl and Kármán independently [Prandtl and Tietjens, 1957, p.75] based on Blasius's law of pressure drop for turbulent flows (Blasius, 1911). This frictional term however is assessed to be negligible or at most accountable as a part of drag force for marine structures with wetted surface areas not appreciably greater than frontal projection areas.

A ship resistance formula is developed by dismissing the incident wave field completely and taking only a constant current in the general expression describing combined wave and current forces. For ship-like vessels the wetted surface area is considerably greater than the frontal projection area hence the skin friction drag cannot be neglected. Therefore, the inertia drag term, whose coefficient is manipulated through Newtonian arguments, and the skin friction term are kept together in establishing a formula for the resistance of ships. The well-known problem of the Froude versus Reynolds scaling is resolved in a fundamental way by sacrificing the true partition of these forces but gaining the correct scaling of the total resistance force. Several surface ships and a submarine are considered for testing the predictive capabilities of the resistance formula. Formulas for estimating the inline and lateral forces acting on a ship in presence of a current at an angle are also suggested in closing.

2. Derivation of a general force expression from 1-D momentum equation

An object partially immersed in fluid and piercing above the free

E-mail address: sbeji@itu.edu.tr.

https://doi.org/10.1016/j.oceaneng.2020.108121
Received 18 May 2020; Received in revised form 3 August 2020; Accepted 15 September 2020
Available online 20 October 2020

surface is considered as shown in Fig. 1. For the sake of generality the breadth $b(z)$ and length $l(z)$ of the object are varying functions of the vertical coordinate z; likewise, the bottom of the object is not necessarily sitting on the bed. An incident flow velocity $u(x, z, t)$, which may be unsteady and vertically varying, impinges on the body in the $x-$ direction only. The momentum equation for 1-D flow is

$$\rho\frac{\partial u}{\partial t}+\rho u\frac{\partial u}{\partial x}=-\frac{\partial p}{\partial x}+\frac{\partial \tau_{yx}}{\partial y} \tag{1}$$

where ρ is the fluid density, u the velocity in the $x-$ direction, p the pressure, and τ_{yx} the shearing stress acting in the $x-$ direction normal to the $y-$ direction. As the flow is taken one dimensional the velocity components v and w are tacitly set to zero by assuming their contribution negligible in accord with Froude-Krylov hypothesis, as evoked in (Morison et al., 1950).

Multiply (1) by the volume element $d\mathscr{V}=dxdydz$ and integrate over the object in the $x-$ and $y-$ directions to get

$$\begin{aligned}
&-\left[\int_{-b(z)/2}^{+b(z)/2}\left(\int_{-l(z)/2}^{+l(z)/2}\frac{\partial p}{\partial x}dx\right)dy\right]dz\\
&=\left[\int_{-b(z)/2}^{+b(z)/2}\int_{-l(z)/2}^{+l(z)/2}\rho\frac{\partial u}{\partial t}dxdy\right]dz\\
&+\left[\int_{-b(z)/2}^{+b(z)/2}\left(\int_{-l(z)/2}^{+l(z)/2}\frac{\rho}{2}\frac{\partial(u^2)}{\partial x}dx\right)dy\right]dz\\
&-\left[\int_{-l(z)/2}^{+l(z)/2}\left(\int_{+b(z)/2}^{+\infty}\frac{\partial \tau_{yx}}{\partial y}dy\right)dx\right]dz\\
&-\left[\int_{-l(z)/2}^{+l(z)/2}\left(\int_{-b(z)/2}^{-\infty}\frac{\partial \tau_{yx}}{\partial y}dy\right)dx\right]dz
\end{aligned} \tag{2}$$

where the last two integrals over the left and right semi-surfaces of the object indicate the frictional drag due to shearing stresses acting on the entire surface area of the object. They are identical for an object with xz-plane symmetry. Carrying out the integrals results in

$$\begin{aligned}
&-\left(p_b-p_f\right)b(z)dz\\
&=\rho\frac{\partial u_r}{\partial t}b(z)l(z)dz+\frac{\rho}{2}\left(u_b^2-u_f^2\right)b(z)dz\\
&-\int_{-l(z)/2}^{+l(z)/2}\left[\tau_{yx}(+\infty)-\tau_{yx}(+b(z)/2)\right]dxdz\\
&-\int_{-l(z)/2}^{+l(z)/2}\left[\tau_{yx}(-\infty)-\tau_{yx}(-b(z)/2)\right]dxdz
\end{aligned} \tag{3}$$

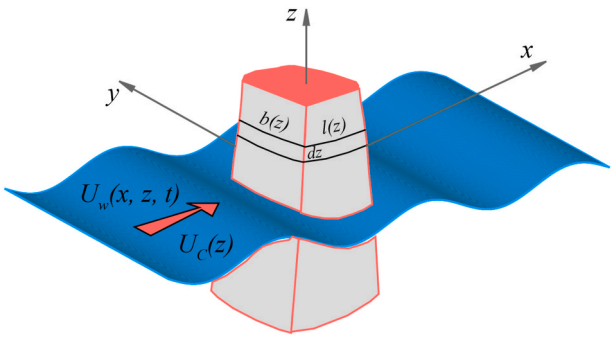

Fig. 1. A pile subjected to waves and currents.

where the subscripts b and f stand respectively for the back and front of the object as aligned in the $x-$ direction.

When the flow is in the positive $x-$ direction the front side pressure p_f is greater than the back side pressure p_b hence p_f-p_b is positive. For a reversed flow direction it is obviously negative. Area element on the front face of the pile $b(z)dz$ is the projected area element $d\mathscr{A}_p(z)=b(z)dz$ of the object facing incident flow. Then, $(p_f-p_b)d\mathscr{A}_p(z)$ indicates the net differential force acting on an infinitesimal height dz of the pile; namely, $dF=(f_f-f_b)dz$, which may be positive or negative depending on the flow direction.

Fluid acceleration $\partial u_r/\partial t$ in the vicinity of the object is calculated by using a *representative* flow velocity u_r, which, for practical purposes, is related to the incident flow velocity by $u_r=C_M u$. Since the accelerative force is associated with the added or virtual mass of moving body the constant C_M may be viewed as an added mass coefficient. The symbol C_M is especially taken to correspond to the mass or inertia coefficient used in (Morison et al., 1950). $b(z)l(z)dz$ is no other than the infinitesimal volume element $b(z)l(z)dz=d\mathscr{V}$ so that the mass force $\rho C_M(\partial u/\partial t)d\mathscr{V}$ is proportional to the *submerged mass* $\rho\mathscr{V}$ of the body.

The second term on the right of Eq. (3) is the so-called *drag force* component of the Morison equation. It is probably more appropriate to name this term *inertia drag* or *dynamic pressure drag* as termed in Prandtl and Tietjens [Prandtl and Tietjens, 1957, p.86–95]. In order to express this component in terms of the incident velocity the difference $u_b^2-u_f^2$ should be related to u^2 by a proportionality factor, say C_D, again as used in (Morison et al., 1950). Writing then $u_b^2-u_f^2=C_D u^2$ gives $\frac{1}{2}\rho C_D u^2 d\mathscr{A}_p(z)$ for the pressure drag per infinitesimal height dz. This term is advective acceleration and it would be wrong to consider the virtual mass force $\rho C_M u_t d\mathscr{V}$ as $\rho C_M(u_t+uu_x)d\mathscr{V}$ to account for total acceleration of the flow field as argued in the relevant literature. It is equally wrong to state that the *linearised* acceleration is used for the flow by taking u_t alone. This misconception arises because the origin of the drag force as given by Morison et al. (1950) could not be traced to the field acceleration uu_x before. With the aid of the present derivation it should be clear that re-introducing uu_x besides u_t in the mass force is erroneous. Such an attempt, as investigated in [14, p.457], reveals a baffling result because the correct way of treating uu_x is to treat it as pressure drag proportional to the *frontal projected area* of the object. Using the total acceleration $\rho(u_t+uu_x)$ for computing inertia force and then adding this to the drag force, which is shown to be arising from ρuu_x, is obviously an inconsistent repetition.

The last two integrals in Eq. (3) represent the frictional force acting on the outer surface of the object. The shearing stresses far away from the surface, $\tau_{yx}(+\infty)$ and $\tau_{yx}(-\infty)$, vanish as the flow field becomes uniform. To proceed with the integrals the shearing stresses on either side of the underwater body surface, $\tau_{yx}(+b(z)/2)$ and $\tau_{yx}(-b(z)/2)$, must be specified. Based on the pressure drop formula of Blasius (1911) from experiments with turbulent flows Prandtl and Kármán, independent of each other, derived the following expression for the shearing stress on a flat plate

$$\tau_0=0.0288\rho u^2\left(\frac{\nu}{u}\right)^{1/5}\frac{1}{\sqrt[5]{x}} \tag{4}$$

where subscript 0 denotes the surface value, u is the undisturbed flow velocity, x the distance in the lengthwise or flow direction along the plate, and $\nu=\mu/\rho$ the kinematic viscosity. Using τ_0 both for $\tau_{yx}(+b(z)/2)$and $\tau_{yx}(-b(z)/2)$, integrating along the length of the object $l(z)$ gives

$$2\int_{-l(z)/2}^{+l(z)/2}\tau_0 dxdz=\left(\frac{0.072}{\sqrt[5]{Re}}\right)\frac{1}{2}\rho u^2\mathscr{C}(z)dz \tag{5}$$

where $Re=ul(z)/\nu$ is the Reynolds number (Reynolds, 1884) computed using the length $l(z)$ in the flow direction x and $\mathscr{C}(z)=2(b(z)+l(z))$ the

perimeter of the object at a height z. It results from the integration of both sides of the object in the $x-$ direction by taking into account the protrusion in the $y-$ direction thus circumscribing the cross-section at height z. Integral $\int \mathscr{C}(z)dz = S_w$ gives the wetted surface area or the underwater surface area of the object. Note that the frictional force for turbulent flow is *not* proportional to u^2 but $u^{9/5} = u^{1.8}$ when the $1/5$th power of velocity in denominator is taken out. Letting $l(z) = L$, Eq. (5) can be rearranged as $(0.036\rho / \sqrt[5]{L/\nu})S_w u^{1.8}$, which is strikingly similar to R. E. Froude's frictional resistance formula $R_F = fS_w U^{1.825}$ with f being a coefficient which depends on the waterline length of the ship [Rawson and Tupper, 2001, p. 699]. Also, these two formulas yield quite comparable quantitative results.

It is possible to use a different shear stress formulation for turbulent flow such as ITTC, ATTC, Hughes or Granville as listed in Lewis [Lewis, 1988, p.12]. Nevertheless, the present work adheres to the Prandtl-Kármán formula as it has a solid theoretical and experimental background.

Now that each contribution in Eq. (2) has been expressed in terms of the incident velocity u, a general expression for the horizontal force dF in the $x-$ direction per infinitesimal height dz can be written as

$$dF = \rho\, C_M \frac{\partial u}{\partial t} d\mathscr{V}(z) + \frac{1}{2}\rho\, C_D u^2 d\mathscr{A}_p(z) + \frac{1}{2}\rho\, C_F u^2\, \mathscr{C}(z)\, dz \tag{6}$$

where $C_F = 0.072\alpha_f / \sqrt[5]{Re}$ is the friction coefficient with an additional constant α_f, which, like C_M and C_D, is introduced to compensate variations in the flow velocity and $O(1)$; for flat plates α_f can simply be set to unity.

A quite important detail concerning the appropriate use of the above formula must be mentioned. The inertia terms, the first two terms, scale according to the Froude number while the remaining friction term scales according to the Reynolds number. If Eq. (6) is to give consistent results for a model and its full-scale, a correction factor must be introduced to the Reynolds number in the friction term. In §6 this problem is resolved by a formal analysis and then demonstrated for a container ship in §6.1.

3. Waves and currents combined

By assuming that the linear superposition principle holds the flow field u may be specified as composed of two different contributions; a steady current $U_c(z)$ which depends only on the vertical coordinate z, such as a logarithmic profile, and an unsteady incident wave field $U_w(x, z, t)$. Thus, letting $u = U_c(z) + U_w(x, z, t)$ in (6) gives

$$\begin{aligned} dF = {} & \rho\, C_M \frac{\partial U_w}{\partial t} d\mathscr{V}(z) + \frac{1}{2}\rho\, C_D \left(U_c^2 + 2U_c U_w + U_w|U_w|\right) d\mathscr{A}_p(z) \\ & + \frac{1}{2}\rho\, C_F \left(U_c^2 + 2U_c U_w + U_w|U_w|\right) \mathscr{C}(z)\, dz \end{aligned} \tag{7}$$

which may be viewed as a generalized form of Morison's equation with an additional term representing the frictional force due to turbulent flow. Absolute values are used to ensure the correct force direction due to cyclic wave motions. We have thus begun with the one-dimensional momentum equation and arrived at a generalized Morison equation without postulating specific forms for the forces involved. Comments on each one of the three terms are now warranted.

The first component is due to local acceleration of the flow field and manifest only for unsteady or time-dependent flows such as waves. This force is proportional to the fluid mass decelerated by a fixed object or accelerated by a moving body.

The second component is due to the advective acceleration of the flow field, which is conventionally called the inertia drag. This force is proportional to the projection area of the object upon which the flow impinges. It is essentially the same as the force caused by a water jet impinging on a plate as shown in Fig. 2. Writing Bernoulli's equation at two different points gives $p = p_{atm} + \frac{1}{2}\rho U^2$ for the pressure on the plate; the force is simply obtained by multiplying the pressure by the circular area on which the jet hits. For a moving body the corresponding resistive force arises from the motion of the body against a motionless inviscid fluid. For a completely submerged symmetrical body one has to deal with D'Alambert's paradox of zero resistance but that may be dismissed as a problem already resolved.

The third component is due to the fluid viscosity which causes a skin friction drag which is proportional to the wetted surface area of the object. Depending on the flow characteristics –laminar, transient, turbulent– the functional dependency of this force on velocity differs. At a first glance the friction drag looks similar to the inertia drag but there are essential differences between the two. First of all, the friction drag is proportional to the wetted surface area of the object whereas the inertia drag to the frontal projection area of the object. More importantly, the skin friction is *not* proportional to the square of the flow velocity but, for this particular turbulence model, to the $9/5$th power of the velocity. Furthermore, C_F is a function of the Reynolds number and when evaluating the total force from Eq. (6) by integration this point must be properly handled. An amendment for the scaling effect as done in §6 must be implemented.

Introduction of the friction drag as a new force component is a notable aspect of the general force expression; however, for structures with relatively small underwater surface areas such as piles, the relative importance of this new term is low compared to the others. For a typical range of Reynolds numbers, $Re = 10^4 - 10^6$, the friction coefficient, $C_F = 0.01 - 0.005$, is quite small; hence, unless the wetted surface area is about one to two orders of magnitude $O(10^1 - 10^2)$ larger than the frontal area, this contribution is negligible. Therefore, the absence of the skin friction term in the Morison equation would not cause any perceptible error, especially as this part could be absorbed into the drag force. On the other hand, ignoring this component in computing the resistance of ship-like forms would simply be unacceptable as demonstrated in §6 by sample resistance computations. Thus, while the absence of skin friction term in certain sea structures is not a problem, its inclusion for vessels with relatively large wetted surface areas is a must. Finally, retaining the skin friction for structures with not quite large but not small wetted surface areas may lead to more refined and accurate force estimates. Accomplishing this aim naturally requires a comprehensive study of re-assessing the quantitative values of C_M, C_D, and C_F. Such a task may possibly be initiated by taking α_f in C_F equal to a definite number such as unity and then investigating the values of C_M and C_D with reference to measurements for varying Reynolds numbers.

4. Morison's equation

Morison, O'Brien, Johnson, and Scaaf (Morison et al., 1950) formulated the total wave force acting on a bottom-mounted surface-piercing pile of circular cross-section as a sum of two contributions: the virtual mass force and the drag force. Since its introduction in 1950 no work of surpassing quality has been reported; therefore, although

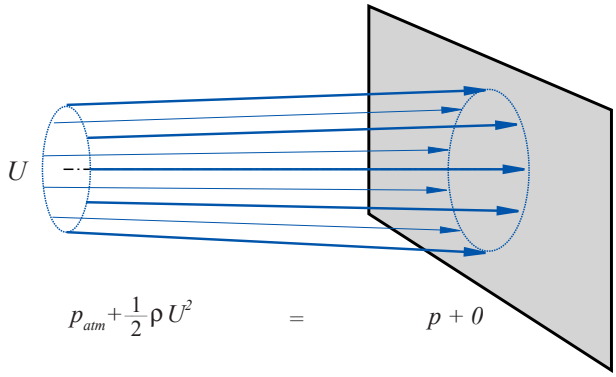

Fig. 2. Water jet impinging on a plate at right angle.

regarded essentially heuristic, it has been in wide use, probably due to the hidden solid foundation behind it. Now that a general expression of total force based on a 1-D momentum equation has been derived the Morison equation can be recovered from it and associated with firm theoretical grounds. In the absence of a current, $U_c = 0$, Eq. (7) becomes

$$dF = \rho\, C_M \frac{\partial U_w}{\partial t} d\mathscr{V}(z) + \frac{1}{2}\rho\, C_D U_w |U_w| d\mathscr{A}_p(z) + \frac{1}{2}\rho\, C_F U_w |U_w|\, \mathscr{C}(z)\, dz \tag{8}$$

The volume and projected area elements for a circular cylinder are $d\mathscr{V}(z) = \frac{\pi}{4}D^2(z)dz$ and $d\mathscr{A}_p(z) = D(z)dz$, respectively. Further, setting the perimeter as $\mathscr{C}(z) = \pi D(z)$ with $D(z)$ denoting the pile diameter at an arbitrary height z, turns Eq. (8) into

$$dF = \frac{\pi}{4}\rho\, C_M \frac{\partial U_w}{\partial t} D^2(z)\, dz + \frac{1}{2}\rho\, C_D U_w |U_w| D(z)\, dz + \frac{\pi}{2}\rho\, C_F U_w |U_w| D(z)\, dz \tag{9}$$

where $C_F = 0.072\alpha_f / \sqrt[5]{Re}$ is the friction coefficient with $Re = U_{wo} D(z)/\nu$ defined in terms of the orbital velocity amplitude U_{wo} and $l(z) = D(z)$. Eq. (9) can be manipulated further by combining the last two terms,

$$dF = \frac{\pi}{4}\rho\, C_M \frac{\partial U_w}{\partial t} D^2(z)\, dz + \frac{1}{2}\rho(C_D + \pi C_F) U_w |U_w| D(z)\, dz \tag{10}$$

If the friction term C_F is dismissed completely or absorbed into C_D, as being small compared to C_D, Eq. (10) becomes Morison's equation in its extended form for vertically varying diameter $D(z)$ as employed in (Beji, 2019).

For oscillatory motions the virtual mass and inertia drag depend on the period or frequency of motion; furthermore, flow irregularities such as separation and vortex shedding appreciably affect the magnitude of these forces. The present formulation, in line with the Morison equation, has ignored such three-dimensional effects completely from the beginning; therefore, it is only natural to lump all these effects into the coefficients. Keulegan-Carpenter number $K = UT/D$ (Keulegan and Carpenter, 1958) and Reynolds number (Reynolds, 1884) are the primary parameters that C_M, C_D, and C_F depend on. For an explicit representation of these dependencies Eq. (10) is re-written as

$$dF = \frac{\pi}{4}\rho\, \tilde{C}_M(K, Re) \frac{\partial U_w}{\partial t} D^2(z)\, dz + \frac{1}{2}\rho\, \tilde{C}_D(K, Re)\, U_w |U_w| D(z)\, dz \tag{11}$$

where $\tilde{C}_M(K, Re)$ and $\tilde{C}_D(K, Re)$ emphasize the parametric dependencies on K and Re. Reader is directed to Sarpkaya and Isaacson [14, p.93–114] for an extensive exposition of the subject.

5. Resistance formula for ship-like forms based on general expression

Resistance of ship-like forms is now investigated in the light of Eq. (6) by assuming that the resistance experienced by a vessel moving at a speed U is equivalent to the external force acting on a stationary vessel in a fluid flowing with velocity U. If the flow velocity is constant the acceleration is zero hence the first term of Eq. (6) vanishes. We then have the inertia and skin friction drag as the components of total resistance. The inertia drag for inclined planes and curved surfaces is examined in line with Newton's classic treatment, which is recapitulated below. Scaling of skin friction drag is elaborated in §6. Wave making drag which is important for surface vessels cannot be explicitly considered in our treatment but an elementary formulation albeit insufficient is presented at the end of this section. It must be emphasized that only a partial treatment of bow effect is accomplished and that the bow and stern wave interaction is not accounted for at all.

5.1. Newton's resistance law revisited

Newton proposed a quadratic resistance law

$$D_I = \rho\, C' \mathscr{A}_p u^2 \tag{12}$$

where D_I is the inertia drag significant for fluids of small viscosity, $C' = u/u'$ is a proportionality factor denoting the ratio of the speed u of moving object to the velocity u' imparted to the fluid particles coming into contact with the body. ρ and $\mathscr{A}_p$ are respectively the fluid density and the projected frontal area of the object in the direction of flow as defined before. The formula essentially states that the momentum generated per unit time is equal to the resistance force acting on the body. The mass of fluid particles coming into collision with the moving body per unit time is $\rho\mathscr{A}_p u$. Velocity u', which is assumed to be proportional to the speed u of the object is imparted to particles. The generated momentum is then $\rho\mathscr{A}_p u u' = \rho C' \mathscr{A}_p u^2$, which is the resistance force experienced by the body. Newton extended the formulation to the case of a flow with an angle β to a perfectly smooth plane. Assuming that the velocity component perpendicular to the plane is *annihilated*, the mass flow rate becomes $\rho\mathscr{A}_p u \sin\beta$ while the imparted velocity is $u \sin\beta$. Consequently, the force acting perpendicular to the plane is $\rho\mathscr{A}_p u^2 \sin^2\beta$ [11, p.86]. These arguments, though speculative in nature, are used in re-defining the inertia drag coefficient C_D for ship-like forms with curved bow shapes.

Unfortunately, resistance force values based on Newton's *impact theory* turned out to overestimate the measurements. For instance if the flow is perpendicular to a plane $\beta = \pi/2$ hence $\sin^2(\pi/2)$ is 1.00, but the experimental value is 0.55. Similar overestimates are observed for different forms [11, p.87]. Despite these discrepancies the quadratic form is in accord with the inertia drag though not strictly valid for the skin friction.

5.2. Shape factor

A simple geometrical form crudely resembling the bow section of a ship with two incident water jets is shown in Fig. 3.

The water jet impinging on the inclined surface is assumed to reflect from it by making the same angle with the surface normal. The reflected jet is resolved into two components; one is running parallel to the inclined surface and other normal to it. Thus, the velocity component normal to the inclined surface is the *annihilated* velocity component in Newton's argument hence responsible for producing a pressure force on the surface as in the case of a water jet hitting on a plane in Fig. 2 with the difference that the velocity normal to the surface is now $U\sin\beta$. The dynamic pressure acting on the inclined plane is then $\frac{1}{2}\rho U^2 \sin^2\beta$and the total force on the inclined surface is $\frac{1}{2}\rho\mathscr{A}U^2\sin^2\beta$ with $\mathscr{A}$ being the surface area. But this force acts normal to the inclined plane, the force acting in the direction of incoming flow is

$$f_i = \left(\frac{1}{2}\rho\mathscr{A}U^2\sin^2\beta\right)\sin\beta = \frac{1}{2}\rho\mathscr{A}_p U^2 \sin^2\beta \tag{13}$$

where $\mathscr{A}_p = \mathscr{A}\sin\beta$ is the projected surface area of the inclined plane. With the exception of the factor $1/2$ Eq. (13) is in complete accord with Newton's formulation for inclined planes. The factor $1/2$, which is an important correction for the magnitude, arises from the use of Bernoulli's equation instead of momentum approach.

Eq. (13) could be obtained in a slightly different way. If we consider that while the normal velocity component $U\sin\beta$ is *annihilated* or reflected away from the surface, the incident flow U continues flowing as $U\cos\beta$ over the inclined surface as shown in Fig. 3, Bernoulli's equation

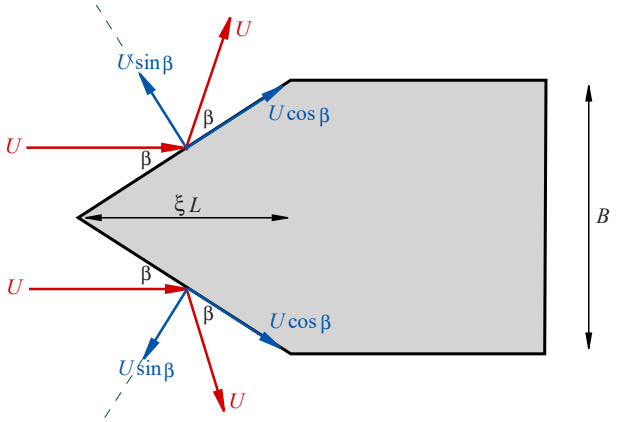

Fig. 3. Water jets impinging on inclined plates of bow-like shape.

written along this flow line is

$$\frac{1}{2}\rho\, U^2 = \frac{1}{2}\rho\, (U\cos\beta)^2 + p_s \tag{14}$$

where p_s is the pressure on the inclined surface and the atmospheric pressure has been dismissed as being immaterial for the present purposes. Solving for p_s gives as before $\frac{1}{2}\rho U^2\sin^2\beta$ for the dynamic pressure on inclined surface.

The presence of a free surface, which could not be included in our formulation, is now partially considered for a flow with velocity U hitting on a curved bow-like form as depicted in Fig. 4. The dynamic pressure on the bow-like solid surface would cause an elevation of the free surface proportional to $U^2\sin^2\beta_l$ with respect to a reference level z_r. Implementing Bernoulli's equation again for an *annihilated* velocity $U\sin\beta_l$ gives

$$\frac{1}{2}\rho\, U^2\sin^2\beta_l + \rho g z_r = 0 + \rho g(z_r + \zeta) \tag{15}$$

where g is the gravitational acceleration, β_l the local inclination angle of the solid surface, and ζ the free surface elevation increase due to the local dynamic pressure. Solving for ζ yields

$$\zeta = \frac{U^2\sin^2\beta_l}{2g} \tag{16}$$

which may be included as a small correction in computing the projected area where the dynamic pressure acts on. This expression of ζ is the only part of the present formulation that can come close to but definitely not sufficient of modelling the wave making drag. Note that the magnitude of ζ gets larger for β_l values approaching the right angle and becomes maximum for $\beta_l = \pi/2$, which corresponds to a jet directly hitting a flat plate as in Fig. 2. On the other hand, ζ gets smaller for smaller β_l values and vanishes completely for $\beta_l = 0$ as sketched in Fig. 4 with blue line.

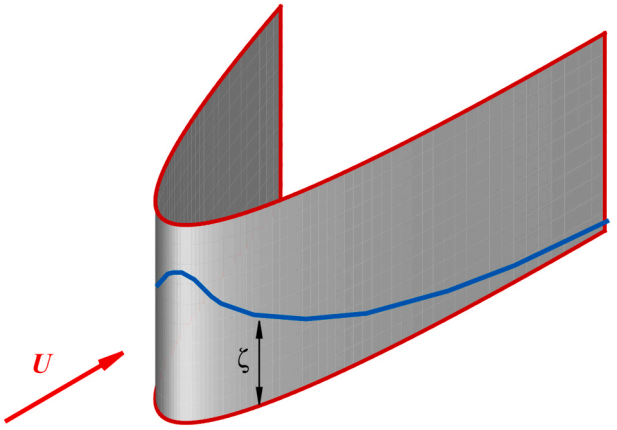

Fig. 4. Free surface elevation ζ (blue) due to a flow impinging on a bow-like shape. (For interpretation of the references to colour in this figure legend, the reader is referred to the Web version of this article.)

The mean inclination angle for any given bow shape can be formulated in terms of a fraction ξ of the ship length L and breadth B. If the distance to the location where the ship breadth reaches its maximum value is ξL, as in Fig. 3, the mean inclination angle would exactly be $\beta = \arctan(B/2\xi L)$, regardless of the precise shape of the bow. Thus,

$$\sin^2\beta = \frac{1}{1 + (2\xi L/B)^2} \tag{17}$$

where the ratio $\xi \leq 1/2$ in general and $\xi = 1/2$ for a ship without parallel body if B is gained exactly at the amidships. ξ may be termed as the bow shape factor of inertia resistance or shortly the shape factor. Nevertheless, this geometrical interpretation should not be taken strictly applicable as the arguments pictured in Figs. 3 and 4 are obviously very speculative. $\sin^2\beta$ should in general be viewed as a multiplier representing the effect of streamlining of the entire body form not only the bow section.

5.3. Specification of shape factor

The selection of ξ is quite important and a definite guidance must be provided for it. First of all, while this parameter stems from entirely geometric considerations of the bow shape it has the wider aspect of covering general hydrodynamic aspects hence resistance characteristics of the ship. Variation range of the shape parameter is found to be relatively limited, $\xi = 0.30 - 0.45$, for different surface ship types including a submarine. Specifically, for a container ship and a fishing vessel $\xi = 0.45$, for a passenger-cargo ship $\xi = 0.35$, for two other ships not reported here $\xi = 0.30$, and finally for a submarine $\xi = 0.35$ agree well with experimental data. This narrow range of change is probably desirable to obtain a good estimate for the resistance curve of a given ship. On the other hand, further parametrization of ξ does not seem possible due principally this limited range of variation. Also, again because of this narrowness in range, the shape factor appears to represent those details in a ship form that cannot be formulated in terms of general parameters such as L, B, T, C_B, etc. In a sense ξ is an ultimate quantity representing the degree of success of a design. If ξ is relatively low, the ship has inefficient resistance characteristics as $\xi = 0$ gives $\beta = \pi/2$, flow hitting at right angle on a flat plate. On the contrary if ξ is higher the ship may be said to be a relatively efficient design.

6. Ship resistance calculations

For a constant current speed U integrating Eq. (6) vertically results in

$$F = \frac{1}{2}\rho\, C_D \mathscr{A}_p U^2 + \frac{1}{2}\rho\, C_F \mathscr{S}_w U^2 \tag{18}$$

where $\mathscr{A}_p$ is the frontal projected area and $\mathscr{S}_w$ the wetted surface area of the vessel. Based on the arguments advanced in §5 the inertia drag coefficient C_D is re-defined to comply with Eq. (13) so that $C_D = \alpha_d\sin^2\beta$, where α_d is constant of $O(1)$ and β the mean inclination angle of the bow form as expressed in Eq. (17). Making use of the new definition of C_D in Eq. (18) and re-arranging result in

$$F = \frac{1}{2}\rho\, \alpha_d \sin^2\beta\left(1 + \frac{B}{\mathscr{A}_p}\frac{\sin^2\beta}{2g}U^2\right)\mathscr{A}_p U^2 + \frac{1}{2}\rho\, \alpha_f\left(\frac{0.072}{\sqrt[5]{Re}}\right)\mathscr{S}_w U^2 \tag{19}$$

in which $Re = UL/\nu$. An effective projected frontal area $\mathscr{A}_{pe} = \mathscr{A}_p + B\zeta = \mathscr{A}_p(1 + B\zeta/\mathscr{A}_p)$ is employed by the use of (16) to account for the additional area due to mean surface rise.

The inertia drag and the skin friction drag are distinctly different parts of the total drag and while the former obeys the Froude scaling law the latter the Reynolds scaling law. Since it is not possible to satisfy these laws simultaneously the Froude scaling is used for the model tests of resistance and the effect of unsatisfied Reynolds scaling is eliminated by a roundabout approach. Likewise, Eq. (19) sums the two different drag components and obviously would not give the correct results for a ship and its model when the same coefficients, α_d, α_f, and ξ, are used in computations. This drawback may be overcome by resorting to the fundamentals. According to the Froude scaling, $U_s/\sqrt{gL_s} = U_m/\sqrt{gL_m}$ so that if $L_s = \lambda L_m$ then $U_s = \lambda^{1/2}U_m$, $\mathscr{A}_{ps} = \lambda^2\mathscr{A}_{pm}$, etc. Assuming that Eq. (19) is given for a full-scale mother ship and we would like to express it in terms of the model ship scaled down by λ, the equation becomes

$$F_s = \frac{1}{2}\rho\,\alpha_d \sin^2\beta\left(1+\frac{\lambda B_m}{\lambda^2\mathscr{A}_{pm}}\frac{\sin^2\beta}{2g}\lambda U_m^2\right)\lambda^2\mathscr{A}_{pm}\lambda U_m^2 + \frac{1}{2}\rho\,\alpha_f\left(\frac{0.072}{\sqrt[5]{\lambda^{1/2}U_m\lambda L_m/\nu}}\right)\lambda^2\mathscr{S}_{wm}\lambda U_m^2 \tag{20}$$

Dividing the entire equation by λ^3 gives

$$\frac{F_s}{\lambda^3} = F_m = \frac{1}{2}\rho\,\alpha_d \sin^2\beta\left(1+\frac{B_m}{\mathscr{A}_{pm}}\frac{\sin^2\beta}{2g}U_m^2\right)\mathscr{A}_{pm}U_m^2 + \frac{1}{2}\rho\,\alpha_f\left(\frac{0.072}{\sqrt[5]{\lambda^{3/2}U_mL_m/\nu}}\right)\mathscr{S}_{wm}U_m^2 \tag{21}$$

The Reynolds number in the skin friction term must obviously be multiplied by $\lambda^{3/2}$ if the force scaling is to be correct. λ may be defined by virtually any dimensional quantity characterizing the ship such as $\lambda = L_s/L_m$, $\lambda = B_s/B_m$, etc. Here, we shall use $\lambda = (\nabla_s/\nabla_m)^{1/3}$ since the displacement volume $\nabla = LBTC_B$ embodies all the basic characteristics of a ship and therefore appears to be a better choice. In order to implement this scale correction into Eq. (21) a definite reference value for ∇_s must be selected. A convenient choice would be to set it to unit cubic meters $\nabla_s = \nabla_{ref} = 1\ \mathrm{m}^3$ so that $\lambda = 1/\nabla_m^{1/3}$ hence $\lambda^{3/2} = \nabla_m^{-1/2}$. It must be emphasized that this multiplier is *non-dimensional* because the reference value is taken dimensional in cubic meters and more importantly by definition λ is a non-dimensional quantity. In principle any dimensionally correct parameter with any reference magnitude can be used; the choice only affects the numerical value set to the shape factor ξ. The true partitioning of the inertia and friction drag is obviously lost unless $\nabla = \nabla_{ref}$ but the total is correct and scaled correctly.

Instead of the Prandtl-Kármán formula, if the more common ITTC approximation is used, the scale corrected friction coefficient becomes $C_F = 0.075/[\log(Re/\sqrt{\nabla}) - 2]^2$ with ∇ being the displacement volume but regarded non-dimensional. ITTC formula gives somewhat higher skin friction drag in comparison with the Prandtl-Kármán formula.

Now that the appropriate scaling has been established for the friction drag component the total resistance experienced by a ship advancing at the constant speed U can be written as

$$\frac{F}{\frac{1}{2}\rho\,\mathscr{A}_pU^2} = \left(1+\frac{B}{\mathscr{A}_p}\frac{\sin^2\beta}{2g}U^2\right)\sin^2\beta + 0.072\left(Re\Big/\sqrt{\nabla}\right)^{-1/5}\left(\mathscr{S}_w/\mathscr{A}_p\right) \tag{22}$$

where the constants α_d and α_f both have been set to unity as the shape factor ξ alone is sufficient to tune the formula. The frontal projection area is calculated as the mean cross-sectional area of the ship $\mathscr{A}_p = \nabla/L = BTC_B$. In case the wetted surface area is unavailable, Taylor's formula $\mathscr{S}_w = c\sqrt{\nabla L}$ with $c = 2.6$ is a good approximation [Stokoe, 2003, p.27].

Eq. (22) has been derived entirely based on the first principles. The main assumption is that the flow is one-dimensional and undisturbed by the presence of the object in accord with the Froude-Krylov hypothesis. A rather speculative argument in line with Newton's momentum approach is also called forth to introduce a tuning parameter for the inertia drag. Addition of the separate contributions of the inertia and friction forces is justified on a firm theoretical foundation by taking into account the scaling appropriately. With the scaling correction Eq. (22) can produce the resistance curves of a parent ship and its model in complete agreement with each other without changing the shape factor ξ, the sole tuning parameter of the equation. This point is demonstrated for a container ship and its model in §6.1.

Resistance curves for three different ships and a submarine are now produced by employing Eq. (22) together with (17). Each curve is then compared with the data points obtained from corresponding experimental measurements. A subsection outlining the use of Eq. (22) for estimating forces due to a current flowing at an angle to a ship is also included.

6.1. Resistance curves of a container ship model and her full-scale

The first test case considered is a ship model of the Korea Research Institute of Ships and Ocean Engineering (KRISO) container ship model MOERI-KCS (Van et al., 1998). The model was introduced solely for research aims and since then it has been used mainly for CFD validation purposes. Here, resistance curves for the model ship and her intended full-scale are computed from Eq. (22) for exactly the same shape factor ξ and compared with experimental data. Table 1 gives the main characteristics of the MOERI-KCS container ship model and the corresponding full-scale ship.

Seawater density and viscosity are taken $\rho = 1026\ \mathrm{kg/m^3}$ and $\nu = 1.189\times10^{-6}\ \mathrm{m^2/s}$, respectively. The corresponding values for fresh water are $\rho = 998.2\ \mathrm{kg/m^3}$ and $\nu = 1.003\times10^{-6}\ \mathrm{m^2/s}$. By trial-and-error the shape factor is set to $\xi = 0.45$ so that $\sin^2\beta = 1/[1+(2\xi L/B)^2] = 0.0236$ both for the model and full-scale ship since $L/B = 7.2786/1.019 = 230.0/32.2 = 7.14$ is the same. The mean projected area is obtained from $\mathscr{A}_p = \nabla/L$ for each case. Unless indicated otherwise the length between perpendiculars L_{pp} is used for all the calculations presented in this and other subsections.

Fig. 5 shows the experimental data and the resistance curve computed from Eq. (22) for a range of Froude numbers $Fr = U/\sqrt{gL}$. Using the same shape factor the resistance curve of the full-scale ship is also computed and drawn in Fig. 6 with scaled up experimental data. Except for minor differences due to the use of different (fresh vs salt water) viscosity values the computed resistance curves are identical. This proves that the different scales are handled perfectly by Eq. (22), which is made up of two distinct drag components with different scaling laws. Provided that the single tuning parameter ξ is selected properly the present resistance formula performs well; disagreement in the high speed region, $Fr > 0.25$, is likely to be a manifestation of additional wave resistance, which could not be included in Eq. (22). From the mathematical point of view Eq. (22) is essentially a second-order polynomial in U but the experimental curve for higher speeds obviously diverges from the quadratic form.

Table 1
Main characteristics of MOERI-KCS container ship model and her full-scale.

	Model	Full-scale
L_{WL} Length waterline	7.3577 m	232.5 m
L_{PP} Length perpendiculars	7.2786 m	230.0 m
B Breadth moulded	1.0190 m	32.2 m
T Draft moulded	0.3418 m	10.8 m
S_W Wetted surface area	9.4379 $\mathrm{m^2}$	9424.0 $\mathrm{m^2}$
∇ Volumetric displacement	1.6490 $\mathrm{m^3}$	52030.0 $\mathrm{m^3}$
C_B Block coefficient	0.6505	0.6505

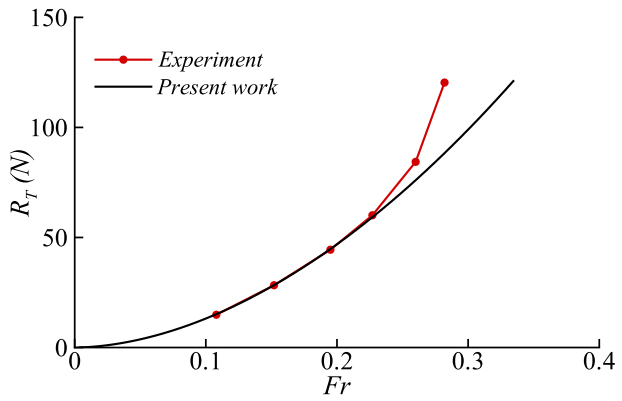

Fig. 5. Resistance curves for MOERI-KCS container ship model. Experimental data (circled red line) and Eq. (22) for $\xi = 0.45$ (black line). (For interpretation of the references to colour in this figure legend, the reader is referred to the Web version of this article.)

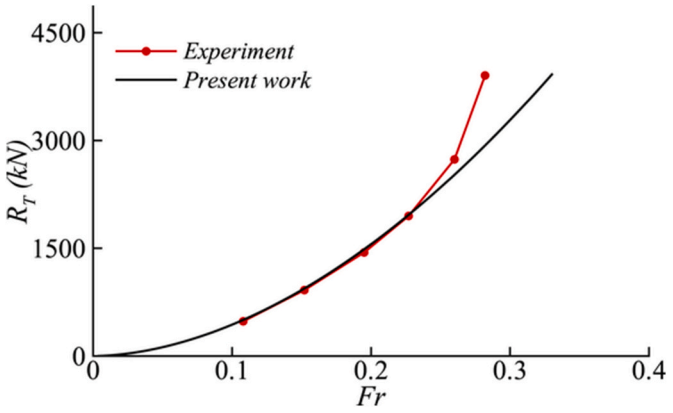

Fig. 6. Resistance curves for MOERI-KCS full-scale container ship. Experimental data (circled red line) and Eq. (22) for $\xi = 0.45$ (black line). (For interpretation of the references to colour in this figure legend, the reader is referred to the Web version of this article.)

6.2. Resistance curve of a fishing vessel

Obreja et al. (2010) investigated the manoeuvring characteristics of a fishing vessel *Città di Genova* and besides hydrodynamic derivatives presented experimental results of resistance tests. The full-scale main characteristics of this vessel are given in Table 2. The wetted surface area is estimated by the use of Taylor's formula $\mathscr{S}_w = 2.6\sqrt{\nabla L}$ and the mean projected area is calculated from $\mathscr{A}_p = \nabla/L$ as indicated before. The shape factor is again set to $\xi = 0.45$ as in §6.1. Despite the very different ship types, the container ship and fishing vessel, the reasonable performance of Eq. (22) with the same $\xi = 0.45$, shown in Fig. 7, may be attributed to two main reasons. First, Eq. (22) contains all the essential elements of expressing ship resistance in terms of overall characteristics of a ship. Second, ξ is not related to the type of ship considered but possibly dependent on the ship form details that cannot be parametrized easily. These points render the determination of ξ for a given ship an open question. A plausible approach is to generate two curves corresponding to, say $\xi = 0.25$ and $\xi = 0.50$, to describe a wide region between higher and lower resistance curves that would include the true resistance curve of the vessel.

Table 2
Main characteristics of fishing vessel *Città di Genova*.

L_{OA} Length overall	32.70 m
L_{PP} Length perpendiculars	25.00 m
B Moulded breadth	8.00 m
T Mean draft	2.58 m
∇ Volumetric displacement	296.00 m^3
C_B Block coefficient	0.574
U Ship speed	12.00 kn

Finally, we must point out that despite the overall acceptable agreement for $\xi = 0.45$, different character of the experimental resistance curve does not allow a good fit in any part. Indeed, a best-fit to the experimental data in the form $R_T = A{\cdot}U^{\alpha}$ yields $A \simeq 0.025$ and $\alpha \simeq 3.07$, revealing that the experimental resistance curve is cubic in U. This remarkable point is not peculiar to this particular case alone and should be investigated on its own, probably in connection with wave-making drag.

6.3. Resistance curve of a passenger-cargo coaster

Hetharia, de Fretes and Gaspersz (Hetharia et al., 2019) studied resistance characteristics of three different ships by computing the resistance curves from statistical formulas and by testing the ship models in towing tank. A passenger-cargo coaster, whose particulars are given in Table 3, is considered here.

Since the length between perpendiculars was not provided an estimated value $L_{PP} = 35.00$ m is used. The shape factor is set to $\xi = 0.35$, lower than the value used in the previous two cases. Fig. 8 shows the resistance curves of the coaster according to the experimental data and Eq. (22). Agreement between the two curves is quite acceptable, especially if allowances are made for the simple form of Eq. (22) with just single tuning parameter ξ.

6.4. Resistance curve of a submarine

DARPA-SUBOFF submarine model developed under the Submarine Technology Program Office of the US Defense Advanced Research Projects Agency (DARPA) is a well-known prototype used for research purposes. Table 4 gives the main characteristics of the DARPA-SUBOFF bare hull submarine model.

Experimental measurements of Han-Lieh and Thomas (1998) are now used for testing the performance of a slightly reduced form of Eq. (22). In the absence of a free-surface the additional increase of the frontal projected area $B\zeta$ is dismissed hence for an underwater vessel Eq. (22) is reduced to the following form.

$$\frac{F}{\frac{1}{2}\rho\,\mathscr{A}_p U^2} = \sin^2\beta + 0.072\left(Re\Big/\sqrt{\nabla}\right)^{-1/5}\left(\mathscr{S}_w\Big/\mathscr{A}_p\right) \tag{23}$$

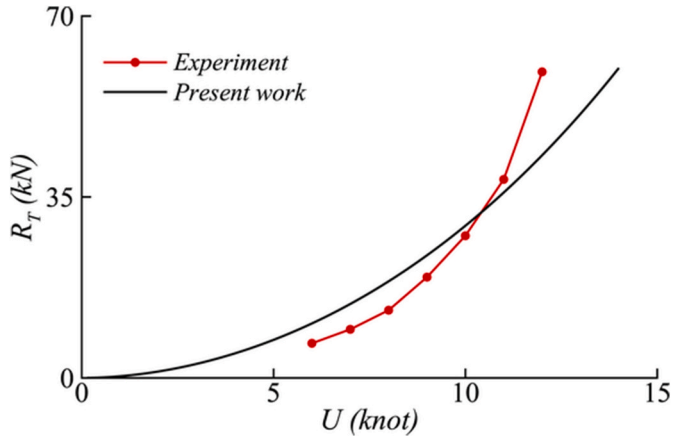

Fig. 7. Resistance curves for fishing vessel *Città di Genova*. Experimental data (circled red line) and equation (6) for $\xi = 0.45$ (black line). (For interpretation of the references to colour in this figure legend, the reader is referred to the Web version of this article.)

Table 3
Main characteristics of passenger-cargo coaster.

L_{OA} Length overall	38.00 m
L_{WL} Length waterline	36.90 m
B Moulded breadth	8.00 m
T Draft	2.50 m
S_W Wetted surface area	327.20 m^2
∇ Volumetric displacement	331.80 m^3
C_B Block coefficient	0.450
U Ship speed	12.00 kn

where $\sin^2\beta = 1/[1+(2\xi L/B)^2]$ as defined before. For constructing the resistance curve of DARPA-SUBOFF model, Eq. (23) is used with $\xi = 0.35$. The fresh water density and viscosity values are used and the projected area is calculated from $\mathscr{A}_p = \nabla/L$ by setting $L = L_{OA}$ for the submarine length.

Fig. 9 shows the resistance curves of DARPA-SUBOFF submarine model according to the experimental data and Eq. (23) for $\xi = 0.35$. The prediction agrees virtually perfectly with the measurements; this must be basically due to the second-order character of the experimental data. We may also conclude that the absence of additional wave making resistance makes the agreement remarkably well; otherwise, above a definite threshold speed, the presence of free-surface changes the character of resistance curve to the third-order.

6.5. Forces due to a current at an angle to a ship

Especially for ship manoeuvring simulations the estimation of wave and current forces at an angle to the ship is of primary importance. Eq. (22) developed for the purpose of estimating ship resistance may well be adopted for such use. Here, we shall outline the basic approach for such a possibility, a detailed investigation exceeds the limits of this already lengthy treatment. Let it be remarked that for wave forces the unsteady mass or inertia force in (7) should be added to (22) while the friction drag can be neglected.

The current angle of attack relative to the bow is expressed as $\gamma_c = \psi - \beta_c - \pi$ where ψ is the heading angle of the ship and β_c the current direction angle measured due north [Fossen, 2011, p.153]. Accordingly, the current velocity components in the $x-$ and $y-$ directions of a co-ordinate system fixed to the ship are $u_c = -V_c\cos\gamma_c$ and $v_c = V_c\sin\gamma_c$ where V_c is the current speed. If the vessel is in motion the relative current speeds $u_r = u - u_c$ and $v_r = v - v_c$ must be used [Fossen, 2011, p.125–27]. Then, in terms of relative current speeds the external force components can be formulated from Eq. (22) as follows.

$$\frac{F_x}{\frac{1}{2}\rho\,\mathscr{A}_{px}u_r|u_r|} = \left(1+\frac{B}{\mathscr{A}_{px}}\frac{\sin^2\beta_x}{2g}u_r^2\right)\sin^2\beta_x + 0.072\left(Re_x\Big/\sqrt{\nabla}\right)^{-1/5}\left(\mathscr{S}_w/\mathscr{A}_{px}\right) \tag{24}$$

$$\frac{F_y}{\frac{1}{2}\rho\,\mathscr{A}_{py}v_r|v_r|} = \left(1+\frac{L}{\mathscr{A}_{py}}\frac{\sin^2\beta_y}{2g}v_r^2\right)\sin^2\beta_y + 0.072\left(Re_y\Big/\sqrt{\nabla}\right)^{-1/5}\left(\mathscr{S}_w/\mathscr{A}_{py}\right) \tag{25}$$

Table 4
Main characteristics of DARPA-SUBOFF submarine model.

L_{OA} Length overall	4.356 m
B Breadth	0.508 m
S_W Wetted surface area	5.980 m^2
∇ Volumetric displacement	0.697 m^3

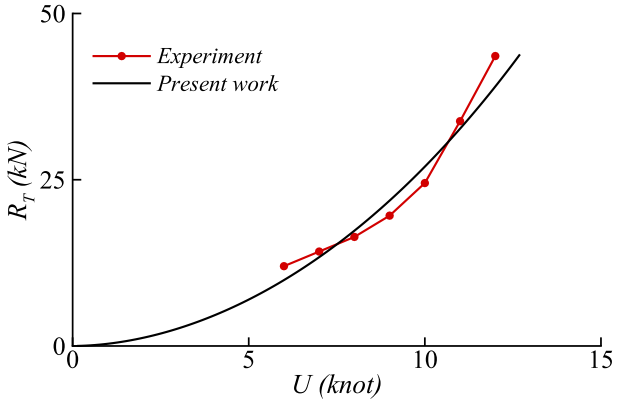

Fig. 8. Resistance curves for a passenger-cargo coaster. Experimental data (circled red line) and Eq. (22) for $\xi = 0.35$ (black line). (For interpretation of the references to colour in this figure legend, the reader is referred to the Web version of this article.)

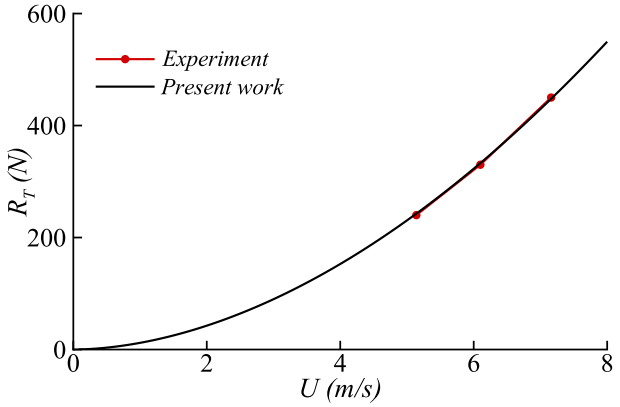

Fig. 9. Resistance curves for DARPA-SUBOFF submarine model. Experimental data (circled red line) and Eq. (23) for $\xi = 0.35$ (black line). (For interpretation of the references to colour in this figure legend, the reader is referred to the Web version of this article.)

In the above formulas $\mathscr{A}_{px} = \nabla/L = BTC_B$ and $\mathscr{A}_{py} = \nabla/B = LTC_B$ are the mean cross-sectional areas in the lengthwise and lateral directions of the ship. The Reynolds numbers for the $x-$ and $y-$ directions are $Re_x = |u_r|L/\nu$ and $Re_x = |v_r|B/\nu$, respectively. $\sin^2\beta_x = 1/[1+(2\xi_x L/B)^2]$ and $\sin^2\beta_y = 1/[1+(2\xi_y B/L)^2]$ are the inertia force coefficients principally determined by the shape factors ξ_x and ξ_y for the $x-$ and $y-$ directions. ξ_x may be taken as determined according to the resistance characteristics of the ship, which is shown to vary approximately in the range $0.30-0.45$. ξ_y on the other hand must be determined by comparisons with experimental measurements of definite ships or relevant statistical formulas. $u_r|u_r|$ and $v_r|v_r|$ are used instead of u_r^2 and v_r^2 to account for correct force directions. Also, the turning moment acting on the ship due to current can be formulated with the aid of F_y as $M_c = x_{gF_y}F_y$ with x_{gF_y} denoting the distance between the horizontal centre of gravity of ship and the acting point of lateral force F_y. In this approach an empirical expression for x_{gF_y} as a percentage of ship length is necessary. The Munk moment in presence of current should also be accounted for properly. Finally, it is worthwhile to note that Eq. (24) becomes identical with (22) when u_r is equated to the ship speed U.

7. Concluding remarks

An elementary treatment of wave and current forces and ship resistance has been done based on the first principles. A general theoretical

formulation of wave and current forces acting on an object has been accomplished by the use of 1-D momentum equation. The resulting general expression renders Morison's equation as a special case, thus placing this equation on a solid theoretical ground. Furthermore, the precise meaning of the drag force is clarified by observing it to be actually nothing more than the inertia drag or dynamic pressure drag.

The inertia drag coefficient of general expression is then modified for ship resistance calculations by following Newton's arguments. The effect of Froude and Reynolds scaling difference is removed by changing the Reynolds number in a way that the resistance calculations for a ship and her model are consistent for the same tuning factor. The resistance formula is tested for three different types of surface ships and a submarine against the experimental data with quite agreeable results. This work however makes no pretence of proposing a precise formula for resistance calculations but rather of disclosing the essential physical mechanisms that lead to sound quantitative estimates. Further refinements in the formulations may be possible in the future by implementing the hints and suggestions made here, especially concerning the wave-making resistance, bow-stern wave interaction, and more importantly change in resistance curve character of surface ships above a threshold speed. The last issue, apparently not brought up in the relevant literature yet, seems to be the most challenging problem.

CRediT authorship contribution statement

S. Beji: The sole author of the manuscript is responsible for conceptualization, Methodology, Software, Writing - review & editing.

Declaration of competing interest

The author declares that he has no known competing financial interests or personal relationships that could have appeared to influence the work reported in this paper.

References

Beji, S., 2019. Applications of Morison's equation to circular cylinders of varying cross-sections and truncated forms. Ocean. Eng. 187, 106156.
Blasius, H., 1911. The law of similarity applied to friction phenomena (in German). Phys. Z. 12, 1175–1178.
Fossen, T.I., 2011. Handbook of Marine Craft Hydrodynamics and Motion Control. John Wiley & Sons Ltd., West Sussex, United Kingdom.
Froude, W., Froude, R.E., 1888. The Resistance of Ships. Government Printing Office, Washington.
Han-Lieh, L., Thomas, T.H., 1998. Summary of darpa-suboff experimental program data. In: Hydromechanics Directorate, Naval Surface Warfare Center. Carderock Division.
Hetharia, W.R., de Fretes, E.R., Gaspersz, F., 2019. Computational and experimental works on ship resistance. In: The First Maluku International Conference on Marine Science and Technology, IOP Conf. Series: Earth and Environmental Science, 012036.
Keulegan, G.H., Carpenter, L.H., 1958. Forces on cylinders and plates in an oscillating fluid. J. Res. Natl. Bur. Stand. (U.S.) 60–5, 423–440.
Lewis, E.V. (Ed.), 1988. Principles of Naval Architecture, vol. II. The Society of Naval Architects and Marine Engineers, Jersey City, NJ.
Morison, J.R., O'Brien, M.P., Johnson, J.W., Schaaf, S.A., 1950. The forces exerted by surface waves on piles. Petroleum Trans., AIME 189, 149–157.
Obreja, D., Nabergoj, R., Crudu, L., Pacuraru-Popoiu, S., 2010. Identification of hydrodynamic coefficients for manoeuvring simulation model of a fishing vessel. Ocean. Eng. 37, 678–687.
Prandtl, L., Tietjens, O.G., 1957. Applied Hydro- and Aeromechanics. Dover Publications Inc., New York.
Rawson, K.J., Tupper, E.C., 2001. Basic Ship Theory. Butterworth-Heinemann, Oxford.
Reynolds, O., 1884. An experimental investigation of the circumstances which determine whether the motion of water shall be direct or sinuous, and of the law of resistance in parallel channels. Phil. Trans. Roy. Soc. Lond. 174, 935–982.
Sarpkaya, T., Isaacson, M., 1981. Mechanics of Wave Forces on Offshore Structures. Van Nostrand Reinhold Company, New York.
SPM, 1984. Shore Protection Manual., vols. I-II. Costal Engineering Research Center, Department of the Army, U. S. Army Corps of Engineers, Washington, D. C., U. S.
Stokoe, E.A., 2003. Reed's Naval Architecture for Marine Engineers. Adlard Coles Nautical, London.
Van, S.H., Kim, W.J., Yim, G.T., Kim, D.H., Lee, C.J., 1998. Experimental investigation of the flow characteristics around practical hull forms. In: Proceedings of the 3rd Osaka Colloquium on Advanced CFD Applications to Ship Flow and Hull Form Design, Osaka, pp. 215–227.